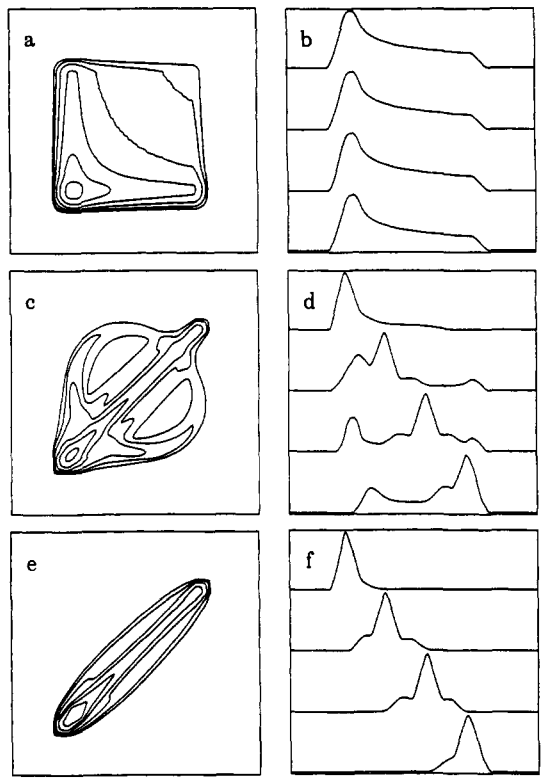

Figure 2. Simulated exchange spectra for $^{13}CH_3OH$ glass with uncorrelated molecular orientations (a,b), α form proposed by Torrie et al. (c,d), and model "β" form with two C-O directions in the unit cell separated by 12° (e,f).

spectra[7,8] indicate that the δ_{33} axis lies within less than 10° of the C-O bond direction. Thus, roughly speaking, the ^{13}C NMR frequency is determined by the angle between the C-O bond and the external field.

Information about molecular orientations *relative to one another* is obtained from two-dimensional NMR exchange[9] experiments on pure $^{13}CH_3OH$. The pulse sequence is 90_{ϕ_1}-t_1-90_{ϕ_2}-τ-90_{ϕ_3}-t_2, with phase-cycling of ϕ_1, ϕ_2, and ϕ_3 to eliminate artifacts and with proton decoupling during t_1 and t_2. In effect, the two-dimensional experiment prepares nuclear spin magnetization on a molecule M_1, measures its NMR frequency f_1 during t_1, transfers the magnetization to nearby molecules M_2 by spin diffusion during τ, and measures their NMR frequencies f_2 during t_2.[10-13] If M_2 has the same orientation as M_1, then $f_1 = f_2$ and the two-dimensional exchange spectrum has intensity only along the diagonal. Otherwise, the spectrum has off-diagonal intensity in a pattern that is determined by the relative orientations of molecules in the unit cell in polycrystalline samples.[10,11]

$^{13}CH_3OH$ (dried over CaH_2, vacuum distilled) was frozen rapidly to form a glass at 103 K, crystallized into the α form by warming to 123 K for 15 min, and converted to the β form by warming to 168 K for 1 h. Figure 1 shows the results of two-dimensional experiments with $\tau = 1$ s on $^{13}CH_3OH$ glass (Figure 1a,b), α-$^{13}CH_3OH$ (Figure 1c,d), and β-$^{13}CH_3OH$ (Figure 1e,f), both as contour plots of the two-dimensional spectra and as series of cross sections through the two-dimensional spectra parallel to the f_1 axis. The spectra of α-$^{13}CH_3OH$ have substantial off-diagonal intensity, in obvious disagreement with the Tauer and Lipscomb structure. Significant off-diagonal intensity is also apparent in the cross sections for β-$^{13}CH_3OH$, again in disagreement with the Tauer and Lipscomb structure (assuming that δ_{33} is along the C-O bond). In parts g and h of Figure 1, the off-diagonal intensity is greatly reduced when spin diffusion is suppressed by diluting $^{13}CH_3OH$ in $^{12}CH_3OH$, indicating that the off-diagonal intensity does not arise from *slow* molecular reorientations.[14,15] The one-dimensional spectrum of the β form (not shown) does show motional averaging, consistent with *rapid* (>10 kHz) librations of methanol molecules about the O-H bond direction with an amplitude of about 30°.[3,16,17]

Figure 2 shows simulated spectra for a methanol glass in which neighboring molecules have uncorrelated orientations (Figure 2a,b), the α structure proposed by Torrie et al. (Figure 2c,d), and a model "β" structure in which there are two molecular orientations in the unit cell with 12° between the C-O bond directions. The simulations assume complete exchange of magnetization during τ and a CSA tensor with δ_{33} along the C-O bond and δ_{22} perpendicular to the C-O-H plane. The good agreement with experiments indicates that the Torrie et al. structure for α-methanol is substantially correct, that there are at least two distinct average C-O bond orientations in the β-methanol unit cell, and that there is apparently no preferred local structure in methanol glass[18] (e.g., the glass is not a defective α form).

(7) Hester, R. K.; Ackerman, J. C.; Neff, B. L.; Waugh, J. S. *Phys. Rev. Lett.* **1976**, *36*, 1081-1083.
(8) Linder, M.; Hohener, A.; Ernst, R. R. *J. Chem. Phys.* **1980**, *73*, 4959-4970.
(9) Jeener, J.; Meier, B. H.; Bachmann, P.; Ernst, R. R. *J. Chem. Phys.* **1979**, *71*, 4546-4553.
(10) Edzes, H. T.; Bernards, J. P. C. *J. Am. Chem. Soc.* **1984**, *106*, 1515-1517.
(11) Henrichs, P. M.; Linder, M. *J. Magn. Reson.* **1984**, *58*, 458-461.
(12) Henrichs, P. M.; Linder, M.; Hewitt, J. M. *J. Chem. Phys.* **1986**, *85*, 7077-7086.
(13) Suter, D.; Ernst, R. R. *Phys. Rev. B* **1985**, *32*, 5608-5627.
(14) Schmidt, C.; Blumich, B.; Spiess, H. W. *J. Magn. Reson.* **1988**, *79*, 269-290.
(15) Blumich, B.; Spiess, H. W. *Angew. Chem., Int. Ed. Engl.* **1988**, *27*, 1655-1672.
(16) Garg, S. K.; Davidson, D. W. *J. Chem. Phys.* **1973**, *58*, 1898-1904.
(17) Denney, D. J.; Cole, R. H. *J. Chem. Phys.* **1955**, *23*, 1767-1772.
(18) Evidence for subtle short-range orientational correlations in the glass may be contained in the dependence of the two-dimensional spectra on τ for $\tau < 1$ s. We are investigating this possibility. At $\tau = 1$ s, the spectra of all three solid forms are fully developed, indicating that spin diffusion has occurred over a distance of several intermolecular spacings.

Electron Propagator Theory of the Ground and Excited States of CaC_5H_5

J. V. Ortiz

Department of Chemistry, University of New Mexico
Albuquerque, New Mexico 87131
Received October 9, 1990

Few ligands appear as frequently in contemporary organometallic chemistry as C_5H_5 and its derivatives. Several spectroscopic[1-3] and theoretical[4,5] studies have shown that radicals composed of group 2 metal atoms and a single ligand with a positive electron affinity have an unpaired electron localized about the positively charged metal atom, coordinated to the anionic ligand. Ab initio electron propagator calculations[6] on the ground and

(1) Nakagawa, J.; Domaille, P. J.; Steimle, T. C.; Harris, D. O. *J. Mol. Spectrosc.* **1978**, *70*, 374. Dulick, M.; Bernath, P. F.; Field, R. W. *Can. J. Phys.* **1980**, *58*, 703. Bernath, P. F.; Field, R. W. *J. Mol. Spectrosc.* **1980**, *82*, 339.
(2) Wormsbecher, R. F.; Trkula, M.; Martner, C.; Penn, R. E.; Harris, D. O. *J. Mol. Spectrosc.* **1983**, *97*, 29. Hilborn, R. C.; Qingshi, Z.; Harris, D. O. *J. Mol. Spectrosc.* **1983**, *97*, 73. Bernath, P. F.; Kinsey-Nielsen, S. *Chem. Phys. Lett.* **1984**, *105*, 663. Bernath, P. F.; Brazier, C. R. *Astrophys. J.* **1985**, *288*, 373.
(3) Ellingboe, L. C.; Bopegedera, A. M. R. P.; Brazier, C. R.; Bernath, P. F. *Chem. Phys. Lett.* **1986**, *126*, 285. Bopegedera, A. M. R. P.; Brazier, C. R.; Bernath, P. F. *Chem. Phys. Lett.* **1987**, *136*, 97. Bopegedera, A. M. R. P.; Brazier, C. R.; Bernath, P. F. *J. Mol. Spectrosc.* **1988**, *129*, 268. Brazier, C. R.; Bernath, P. F. *J. Chem. Phys.* **1988**, *88*, 2112.
(4) Ortiz, J. V. *J. Chem. Phys.* **1990**, *92*, 6728.
(5) Ortiz, J. V. *Chem. Phys. Lett.* **1990**, *169*, 116.
(6) Linderberg, J.; Öhrn, Y. *Propagators in Quantum Chemistry*; Academic Press: New York, 1973. von Niessen, W.; Schirmer, J.; Cederbaum, L. S. *Comput. Phys. Rep.* **1984**, *1*, 57. Herman, M. F.; Freed, K. F.; Yeager, D. L. *Adv. Chem. Phys.* **1981**, *48*, 1. Öhrn, Y.; Born, G. *Adv. Quantum Chem.* **1981**, *13*, 1. Simons, J. In *Theoretical Chemistry: Advances and Perspectives*; Eyring, H., Ed.; Academic Press: New York, 1978.

0002-7863/91/1513-3593$02.50/0

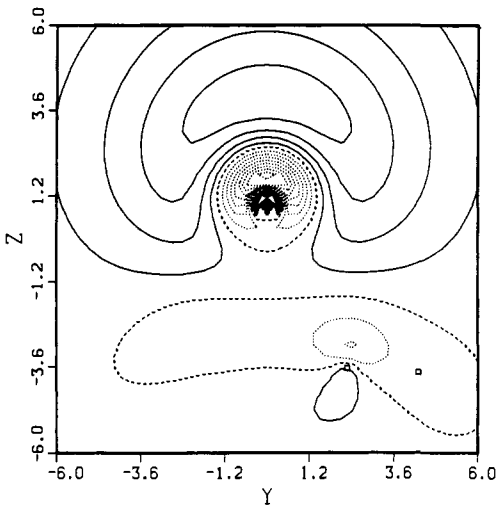

Figure 1. $\tilde{X}^2A_1$ Feynman–Dyson amplitude of CaC_5H_5.

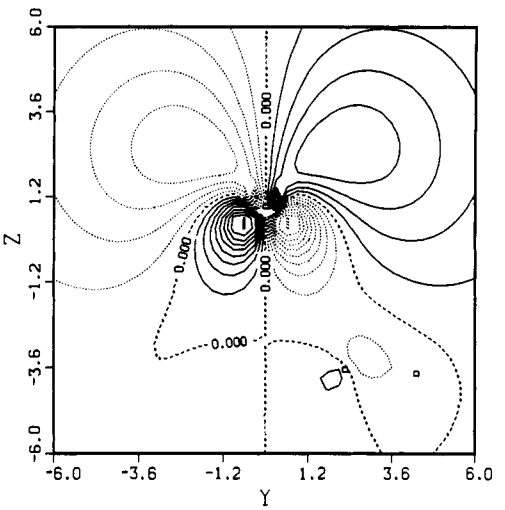

Figure 2. $\tilde{A}^2E_1$ Feynman–Dyson amplitude of CaC_5H_5.

Table I. FDA Expectation Values (Atomic Units)

property	$\tilde{X}^2A_1$	$\tilde{A}^2E_1$	$\tilde{B}^2A_1$	$\tilde{C}^2E_2$
$\langle z \rangle$	3.023	2.817	2.504	0.751
potential at Ca	−0.280	−0.255	−0.322	−0.381
potential at C	−0.137	−0.127	−0.149	−0.182
E_z at Ca	0.041	0.008	−0.001	−0.001
E_z at C	0.015	0.013	0.019	0.021
E_y at C	−0.005	−0.005	−0.007	−0.007

excited states of CaC_5H_5[7] reveal the behavior of the metal-centered electron.

Gaussian 88[8] optimizes CaC_5H_5's Hartree-Fock, C_{5v} geometry with Ca (5s,3p,2d)[4,5,9] and 6-31G(d)[10] for C and H. With the ring frozen in the first geometry, where C–C and C–H are 1.409 and 1.074 Å, respectively, reoptimization of the distance between Ca and the ring centroid with second-order many-body perturbation theory[11,12] proves inconsequential. Ca is separated from the C's by 2.71 Å.[13]

The closed-shell cation being used as a reference state at the neutral's geometry, EPT90[14] calculates correlated electron affinities[15,16] in the nondiagonal second-order, diagonal second-order, and diagonal partial fourth order[17] approximations with a (7s,4p,3d) basis on Ca[18] and 6-31G[10] on C and H. Discrepancies between approximations are 0.15 eV or less. Diagonal second-order results with a larger basis, composed of Ca (8s,5p,4d) and C and H 6-31G(d,p), deviate by less than 0.03 eV. Differences between the diagonal, partial fourth order electron affinities for the neutral ground state (5.078 eV) and excited states provide vertical excitation energies: 1.801 ($\tilde{A}^2E_1$), 2.296 ($\tilde{B}^2A_1$), 2.704 ($\tilde{C}^2E_2$), and 3.143 eV ($\tilde{D}^2A_1$). These agree closely with experimental results[7] for the lowest excited states: 1.800 ($\tilde{A}^2E_{1(1/2)}$), 1.807 ($\tilde{A}^2E_{1(3/2)}$), and 2.208 ($\tilde{B}^2A_1$).

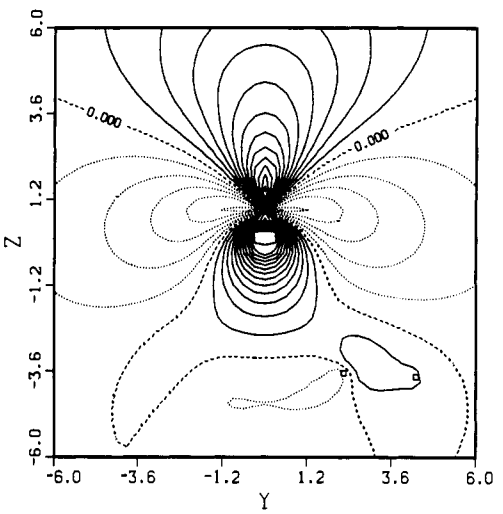

Figure 3. $\tilde{B}^2A_1$ Feynman–Dyson amplitude of CaC_5H_5.

Feynman–Dyson amplitudes (FDAs) for electron affinities of the cationic, N-electron state are defined by

$$\int \Psi^*_N(x_2,x_3,x_4,\ldots,x_{N+1})\Psi_{N+1}(x_1,x_2,x_3,\ldots,x_{N+1})\, dx_2\, dx_3\, dx_4 \ldots dx_{N+1} = \phi^{FDA}(x_1).$$

FDAs are orbitals that correspond to electron binding energies. In the uncorrelated case, the FDA corresponding to the Koopmans's theorem[19] result is a canonical orbital. The present FDAs, calculated in the second-order, nondiagonal approximation, incorporate correlation effects. For the neutral ground state, $\tilde{X}^2A_1$, the FDA contains diffuse Ca s functions with minor p hybridization. In the contour plot (Figure 1), squares represent Ca (0,0,0.929), C (0,2.265,−3.659) and H (0,4.292,−3.761) nuclear positions.[20] This FDA is a Ca 4s–4p hybrid that has been orthogonalized to a ligand π molecular orbital.

The FDA expectation value of z (Table I) reflects polarization away from the ligand. An electron in this nonbonding FDA samples the neighborhood around Ca more than that of any other nucleus. Electric fields evaluated at the nuclei yield another

(7) O'Brien, L. C.; Bernath, P. F. *J. Am. Chem. Soc.* **1986**, *108*, 5017.
(8) Frisch, M. J.; Head-Gordon, M.; Schlegel, H. B.; Ragavachari, K.; Binkley, J. S.; Gonzalez, C.; DeFrees, D. J.; Fox, D. J.; Whiteside, R. A.; Seeger, R.; Melius, C. F.; Baker, J.; Martin, R.; Kahn, L. R.; Stewart, J. J. P.; Fluder, E. M.; Topiol, S.; Pople, J. A. *Gaussian 88*; Gaussian, Inc.: Pittsburgh, PA, 1988.
(9) *Gaussian Basis Sets for Molecular Calculations*; Huzinaga, S., Ed.; Elsevier: Amsterdam, 1984.
(10) Hehre, W. J.; Ditchfield, R.; Pople, J. A. *J. Chem. Phys.* **1972**, *56*, 2257. Clark, T.; Chandrasekhar, J.; Spitznagel, G. W.; Schleyer, P. v. R. *J. Comput. Chem.* **1983**, *4*, 294. Hariharan, P. C.; Pople, J. A. *Theor. Chim. Acta* **1973**, *28*, 213.
(11) Binkley, J. S.; Pople, J. A. *Int. J. Quantum Chem.* **1975**, *9*, 229.
(12) Bartlett, R. J. *Annu. Rev. Phys. Chem.* **1981**, *32*, 359.
(13) A $Ca(C_5H_5)_2$ crystal structure of an η^5-C_5H_5 obtains two values for the Ca–C distance, 2.75 and 2.85 Å. See: Zerger, R.; Stucky, G. *J. Organomet. Chem.* **1974**, *80*, 7.
(14) EPT90, an electron propagator program by J. V. Ortiz, University of New Mexico, 1990.
(15) Ortiz, J. V. *Int. J. Quantum Chem., Quantum Chem. Symp.* **1987**, *No. 21*, 469.
(16) Ortiz, J. V. *Int. J. Quantum Chem., Quantum Chem. Symp.* **1988**, *No. 22*, 431.
(17) Ortiz, J. V. *J. Chem. Phys.* **1988**, *89*, 6348.
(18) The (7s,4p,3d) Ca basis is the same as the (8s,5p,4d) basis of refs 4 and 5 except that the most diffuse s, p, and d functions are omitted.
(19) Koopmans, T. C. *Physica* **1933**, *1*, 104.
(20) Contours in intervals of 0.015 are shown in the figures. Solid (dotted) contours represent positive (negative) values while dashed contours denote nodes.

measure of the FDA's distribution. At Ca and at each C nucleus, z components are positive; the y component at the C in Figure 1 is negative. Multiplication of these values by nuclear charges produces forces in which the ligand nuclei will be drawn upward, but the Ca will be drawn more. Electron interaction more fully screens attractions to the anionic ligand's nuclei than the attraction to the cationic metal atom's nucleus.

Ca d and p functions with π pseudosymmetry constructively interfere away from the ligand (Figure 2) in $\tilde{A}^2E_1$'s FDA. $\langle z \rangle$ is slightly less than in the ground state's FDA. Nuclear attraction energies and forces on the nuclei are weaker, especially for Ca.

$\tilde{B}^2A_1$'s FDA consists chiefly of diffuse d functions on Ca and has small contributions from diffuse Ca p functions. Note the nodal surface (Figure 3) that extends from the Ca nucleus and cuts through the C nucleus. An in-phase relationship obtains between the lower lobe on Ca and functions describing C–H bonding. The smaller $\langle z \rangle$ indicates less polarization away from the ligand. Attraction energies to Ca and C are more negative than in the ground state's FDA. Especially significant is the negative sign of the electric field at the Ca nucleus. All of the forces on the ligand nuclei exceed those of the ground state. This FDA is less antibonding between Ca and C_5H_5 than the other two FDAs.

Ca d functions with δ pseudosymmetry practically alone contribute to the $\tilde{C}^2E_2$ FDA. $\langle z \rangle$ approximates the position of the Ca nucleus. Translation of charge to smaller z accompanies more negative nuclear attraction potentials. Coulombic interactions with the electrons and nuclei of the ligand are larger, but almost no force is exerted on Ca in the z direction for this nonbonding FDA.

The most diffuse Ca s functions are the largest contributors to the FDA of $\tilde{D}^2A_1$. This FDA is primarily a diffuse sp hybrid that has been orthogonalized to functions describing the ligand.

Acknowledgment. An allocation from the Pittsburgh Supercomputer Center facilitated these calculations. This material is based on work supported by the National Science Foundation under Grant No. CHE-8723185.

High Oxygen-Evolving Activity of Rigidly Linked Manganese(III) Porphyrin Dimers. A Functional Model of Manganese Catalase

Yosinori Naruta* and Kazuhiro Maruyama

Department of Chemistry, Faculty of Science
Kyoto University, Sakyo-ku, Kyoto 606, Japan
Received October 24, 1990

Polynuclear manganese complexes[1] play key roles in photosynthetic oxygen evolution[2] and manganese catalase (Mn-CAT).[3] Their functional relevance[4] to oxygen evolution is important both for the structural clarification of oxygen evolving complexes and for the design of their artificial models. One subunit of Mn-CAT from *Thermus thermophilus* contains two Mn^{3+} as an enzymatic active center separated by 3.6 Å.[3d] The enzyme is believed to decompose H_2O_2 by a mechanism that is unimolecular in peroxide and involves Mn^{2+} and Mn^{3+}.[3d,e] Functional modeling of this catalase activity, however, has been simulated only with a single example of a covalently linked binuclear Mn complex.[5]

We have synthesized functional models by linking two manganese porphyrins[6] (**1**, **2b**, and **3**) by rigid linker molecules to control the metal–metal distance and their stereochemistry.

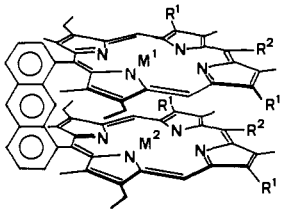

1. $R^1 = n\text{-}C_6H_{13}$, $R^2 = H$, $M^1 = M^2 = Mn^{3+}Cl^-$

2a. $R^1 = n\text{-}C_6H_{13}$, $R^2 = p\text{-}C_6H_4$, $M^1 = H_2$, $M^2 = Mn^{3+}Cl^-$

2b. $R^1 = n\text{-}C_6H_{13}$, $R^2 = p\text{-}C_6H_4$, $M^1 = M^2 = Mn^{3+}Cl^-$

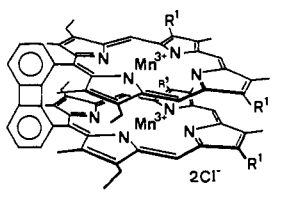

3. $R^1 = n\text{-}C_6H_{13}$

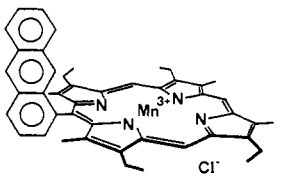

4

These compounds survive more than 10000 turnovers of H_2O_2 in the best case and have a cavity surrounded by porphyrin rings. The catalase activity was measured from three dimanganese complexes (**1**, **2b**, and **3**) and for their corresponding Mn porphyrin monomers [**2a**, Mn(TPP)Cl, and **4**] in a thermostated reaction cell fitted with an oxygen electrode (Table I). In the absence of 1-methylimidazole (MeIm), every Mn porphyrin showed almost no catalase activity. Remarkably, the Mn porphyrin dimers **1** and **2b** showed high oxygen-evolving activity with increased imidazole concentration. **2b** especially attained very high activity [325 mol of O_2 (mol of catalyst)$^{-1}$ min^{-1}] and high turnover numbers (maximum 1.5×10^4). For other Mn porphyrins, MeIm had little or no effect on their catalase activity. By means of spectrophotometric titration, each Mn porphyrin monomer in **1** and **3** forms only the corresponding five-coordinate complex with MeIm.[7] Complexes **1**, **2b**, and **3** have cavities made up of two bulky porphyrins which sterically prevent the entrance of MeIm

Table I. Catalase Activity of Manganese Porphyrins[a]

Mn porphyrin	[MeIm],[b] M	O_2 evolution initial rate, mol min^{-1}	turnover rate, min^{-1}
1	0	0	0
	7.5×10^{-3}	6.2×10^{-6}	10.3
	7.5×10^{-2}	5.4×10^{-5}	90.0
	1.5×10^{-1}	7.5×10^{-5}	125
2a	1.5×10^{-1}	0	0
2b	1.5×10^{-1}	1.8×10^{-4}	325
3	0	0	0
	1.5×10^{-2}	0	0
Mn(TPP)Cl[c]	0	2.4×10^{-7}	0.4
	1.5×10^{-2}	4.0×10^{-6}	1.6
4	0	2.4×10^{-7}	0.40
	1.9×10^{-1}	8.4×10^{-7}	1.40

[a] Conditions: [Mn porphyrin] = 3.75×10^{-4} M (as a porphyrin monomer), $[H_2O_2] = 6.96 \times 10^{-2}$ M in an acetonitrile solution (1.60 mL), $T = 10.0 \pm 0.2$ °C. [b] 1-Methylimidazole. [c] TPP: *meso*-tetraphenylporphyrin.

(1) For recent reviews: Wieghardt, K. *Angew. Chem., Int. Ed. Engl.* **1989**, *28*, 1153–1172. Christou, G. *Acc. Chem. Res.* **1989**, *22*, 328–335.

(2) Dismukes, G. C. *Photochem. Photobiol.* **1986**, *43*, 99–115. Brudvig, G. W. *J. Bioenerg. Biomembr.* **1987**, *19*, 91–142. Pecoraro, V. *Photochem. Photobiol.* **1988**, *48*, 249–264.

(3) *Lactobacillus plantarum*: (a) Beyer, W. F., Jr.; Fridovich, I. *Biochemistry* **1985**, *24*, 6460–6467. (b) Kono, Y.; Fridovich, I. *J. Biol. Chem.* **1983**, *258*, 13646–13648. *Thermus thermophilus*: (c) Allgood, G. S.; Perry, J. J. *J. Bacteriol.* **1986**, *168*, 563–567. (d) Barynin, V. V.; Vagin, A. A.; Melik-Adamyan, V. R.; Grebenko, A. I.; Khangulov, S. V.; Popov, A. N.; Andrianova, M. E.; Vainshtein, A. B. K. *Sov. Phys.—Dokl.* **1986**, *31*, 457–459. (e) Khangulov, S. V.; Voyevodskaya, N. V.; Varynin, V. V.; Grebenko, A. I.; Melik-Adamyran, V. R. *Biophysics* **1987**, *32*, 1044–1051. (f) Khangulov, S. V.; Andreeva, N. E.; Gerasimenko, V. V.; Gol'dfel'd, M. G.; Barynin, V. V.; Grebenko, A. I. *Zh. Fiz. Khim.* **1990**, *64*, 17–27; *Russ. J. Phys. Chem.* **1990**, *64*, 10–16.

(4) Frash, W. D.; Mei, R. *Biochim. Biophys. Acta* **1987**, *891*, 8–14. Wydrzynski, T.; Mano, J.; Takahashi, M.; Asada, K. *Biochemistry* **1987**, *26*, 2495–2501. Ångström, J.; Vänngård, T. *Biochim. Biophys. Acta* **1989**, 973, 23–28.

(5) Mathur, P.; Crowder, M.; Dismukes, G. C. *J. Am. Chem. Soc.* **1987**, *109*, 5227–5233.

(6) Anthracene- and biphenylene-linked porphyrin dimers **1–3** were synthesized by modification of the reported method. Cf.: Chang, C. K.; Abdalmuhdi, I. *Angew. Chem., Int. Ed. Engl.* **1984**, *23*, 164–165.

(7) Formation constants of mono(imidazole) (K_1) and bis(imidazole) complexes(β) at 20 °C: **1**, $K_1 = 1.2 \times 10^4$ M^{-1}, $\beta = 0$ M^{-1}; **4**, $K_1 = 1.6 \times 10^4$ M^{-1}, $\beta = 1.36 \times 10^7$ M^{-1}.

0002-7863/91/1513-3595$02.50/0